IEEE Access
Multidisciplinary | Rapid Review | Open Access Journal

Received 11 October 2023, accepted 22 October 2023, date of publication 30 October 2023, date of current version 8 November 2023.

Digital Object Identifier 10.1109/ACCESS.2023.3328400

RESEARCH ARTICLE

Reliability Assessment of Distributed Network Control System Based on Time Delay Evaluation

LONGHANG HUANG, YING WANG, AND SHENG LIANG
School of Mechanical Engineering, Inner Mongolia University of Technology, Hohhot 010051, China
Corresponding author: Ying Wang (iris.yingwang@outlook.com)

This work was supported by the Natural Science Foundation of Inner Mongolia under Grant 2020MS05005.

ABSTRACT Based on the strict requirements of industrial applications for network real-time and reliability, this paper considers path performance correlation analysis using network delay parameters and evaluates the performance reliability of distributed network control systems (NCSs). The cumulative distribution function of the delay of each information transmission path in the system is constructed, and the reliability of the cluster path is analyzed utilizing multivariate Archimedean Copula functions (ACFs), which describes the path performance correlation, then the fitting effect of Copula function is evaluated by using the squared Euclidean distance method. Finally then the reliabilities of each subsystem and the whole system are calculated full probability formula. To simulate the time delay data of each path in the system, an OPNET-based distributed NCSs simulation platform is established. The reliability of distributed NCSs with 3 sub-systems is evaluated, and the effectiveness of the time delay-based performance reliability evaluation of the distributed NCSs is verified. The results is useful of network parameters optimization and improve the performance reliability of distributed NCS.

INDEX TERMS Distributed networks, reliability, Copula functions, correlation.

I. INTRODUCTION

NCSs are extensively employed across various industries. As the scale of industrial systems continues to grow, the methods for information transmission between nodes have become increasingly intricate and diverse. Furthermore, owing to the functional interdependence of the communication paths and network performance parameters, the system's paths are not entirely independent; they exhibit a certain degree of correlation [1], [2]. Assessing the reliability of such complex distributed NCSs is of paramount importance to ensure their smooth and safe operation.

Numerous scholars have proposed various research methods for the reliability assessment of NCSs. Winfree [3] introduced a top-down approach to network reliability assessment, focusing on flow path information. Rothemund and Winfree [4] developed a method based on the dynamic characteristics of the system, evaluating the probability of operating parameters not exceeding a specific threshold over time. Adleman et al. [5] proposed a congestion-based network performance reliability method. This method uses the ratio of successfully sent packets to the sum of successfully received packets and lost packets as an assessment indicator. However, these methods assume that the performance of each path in the network is entirely independent. Srinivasan et al. [6] were pioneers in confirming the presence of significant correlations in the performance of wireless network paths. These correlations stem from both the inherent interconnections between network paths and the interplay of network performance parameters. Such correlations can have a substantial impact on the evaluation of network performance reliability. As a result of these findings, researchers have delved into the study of path performance correlations within NCSs. Khreishah et al. [7] introduced a distributed chance routing algorithm that incorporates network coding and takes into account path correlations. This approach aims to enhance path performance reliability, particularly in the face of varying delay and packet loss rates within wireless channels. In the realm of anomaly detection systems, where the consequences of a single fault on other network compo-

The associate editor coordinating the review of this manuscript and approving it for publication was Cristian Zambelli.

nents are not always considered, Haylett et al. [8] explored the application of deep learning recurrent neural networks and correlation analysis techniques for system-scale anomaly detection. This approach addresses the need to detect anomalies that might be masked by interdependencies within the network. Recognizing the limitations of existing reliability analysis methods in predicting the effects of changes in component reliability on overall system reliability, Yang et al. [9] proposed an active learning function called 'Expected System Improvement.' This function is designed for system reliability analysis and enables the prediction of how updates in component reliability can impact the reliability of the entire system.

Compared to traditional mechanical structures, network structures exhibit a high degree of complexity and employ various communication methods. This complexity poses challenges in developing comprehensive reliability models that accurately reflect path correlations in rigorous models. In recent years, the use of data-driven system correlation analysis has significantly advanced the field of network reliability, with Copula functions emerging as a valuable tool for assessing performance correlations. Copula functions offer distinct advantages in terms of dimensional reduction and nonlinear data representation for high-dimensional complex datasets. Yuqin et al. [10] employed Copula functions in combination with the non-parametric kernel density method to predict grid reliability indicators. Meanwhile, Liu and Chen [11] utilized the Copula function, employing both kernel density estimation and maximum likelihood estimation, to establish a dynamic reliability model for gearbox systems. Subsequently, they conducted dynamic reliability evaluations for the gearbox. Hai et al. [12] employed copula theory to develop reliability models for mechanical systems, particularly focusing on the intricate interdependencies within series mechanical systems. In the context of NCSs, Zoppi et al. [13] devised a delayed reliability model for NCSs that takes into consideration factors such as network delay and packet loss. Their approach evaluated the impact of loop information transmission success probability on system quality. For an in-depth analysis of network performance concerning specific transmission time requirements, Jian et al. [14] integrated network component reliability models, network topology models, and network performance models. They established a dynamic delay-based network reliability model. Sheng et al. [15] employed a combination of theoretical analysis and data-driven methods and introduced Copula functions to describe the performance reliability of centralized NCSs.

As NCSs continue to expand in scale, evolving into distributed systems where there's no longer a single processing and control center, assessing operational reliability presents new challenges. In this context, the paper proposes a novel approach for evaluating the reliability of distributed NCSs. This approach introduces multivariate ACFs to describe paths, path families, subsystems, and the overall system correlations step by step, all while considering path performance. The network path delay is utilized as an index to evaluate network performance.

II. BASIC THEORY OF THE MULTIVARIATE ACFs

To investigate the reliability calculation method for NCSs based on path performance correlation from a data-driven perspective, we introduce the Archimedes Copula function [16]. Copula functions are a class of mathematical functions that link the joint distribution function to their corresponding marginal distribution functions. They are versatile tools capable of describing various dependencies between random variables, encompassing linear, nonlinear, normal, and non-normal relationships [17]. Copula functions enable the separate modeling of the marginal and joint distributions of a variable. This property allows us to treat the marginal distribution of each variable independently. As a result, we can amalgamate the marginal distribution functions of link delays using the Copula function link function. This, in turn, facilitates the analysis of the reliability of link families, subsystems, and the entire system.

A. MODELING OF THE MULTIVARIATE ACFs

In distributed NCSs, the number of paths within different path families varies, and a central node is often connected to three or more target nodes. Constructing a multivariate ACFs that best captures the correlation among all paths in a multi-path scenario is of utmost importance. Sklar [18] asserted that ACFs exhibits the following characteristics: the ACFs for an N-element system can be effectively represented by binary ACFs, meaning it can be decomposed into (N-1) binary ACFs. For instance, in accordance with the law of ACF combination as described in eq. (1), the ternary ACF can be deconstructed into two binary ACFs.

$$C\left(u_1, u_2, u_3\right) = C\left(C\left(u_1, u_2\right), u_3\right) \tag{1}$$

where u_1, u_2, u_3 are edge distribution functions.

B. SELECTION OF ACFs

In this paper, the selected ACFs encompass the Gumbel Copula function, the Clayton Copula function, and the Frank Copula function. The accurate representation of the relationship between random variables, achieved by selecting the appropriate Copula function tailored to specific scenarios, significantly impacts the final model of the ACF and the subsequent reliability calculations. The binary distribution functions for these ACFs are presented below. The distribution function expression for the binary Gumbel Copula function is detailed as follows.

$$C_G\left(u, v, \alpha\right) = e^{\left(-\left[(-lnu)^{\frac{1}{\alpha}} + (-lnv)^{\frac{1}{\alpha}}\right]^{\alpha}\right)} \tag{2}$$

where $\alpha \in (0, 1]$ is the related parameter and u, v are the edge distribution functions.

The equation for the distribution function of the binary Clayton Copula function as follows.

$$C_{cl}\left(u, v, \theta\right) = max\left(u^{-\theta} + v^{-\theta} - 1\right)^{-\frac{1}{\theta}} \tag{3}$$

where $\theta \in (0, \infty)$ and is the related parameters.

The equation for the distribution function of the binary Frank Copula function as follows.

$$C_F(u, v, \gamma) = -\frac{1}{\gamma} \ln\left(1 + \frac{\left(e^{-\gamma u} - 1\right)\left(e^{-\gamma v} - 1\right)}{\left(e^{-\gamma} - 1\right)}\right) \quad (4)$$

where γ is the related parameter and $\gamma \neq 0$.

This paper employs the squared Euclidean distance, denoted as d_Gu, as an evaluation metric for the optimal Archimedean Copula model. The squared Euclidean distance serves as a fitting index that quantifies the disparity between the empirical Copula function of the sample and the joint distribution function [19]. To compare the fitting performance of the three ACFs, we calculate their respective squared Euclidean distances. The ACF with the smallest squared Euclidean distance is considered to provide the best fit. The following outlines the specific steps in this evaluation process.

a) Estimation of the unknown parameters in the Copula model using the maximum likelihood estimation method under the Copula functional model.
b) The definition of the empirical Copula function of the sample is shown in eq. (5). The alternative Copula function is squared with the empirical Copula function for the squared Euclidean distance d_{Gu}, when d_{Gu} is small, the Copula function fits better, and the model with a minimum value of d_{Gu} is chosen as the optimal Copula model.

$$\hat{C}(u_i, v_i) = \frac{1}{n} \sum_{i=1}^{n} I\left[F(x_i) \leq u_i\right] \cdot I\left[G(y_i) \leq v_i\right] \quad (5)$$

where $F(x_i)$ and $G(y_i)$ are marginal distribution functions, I is an indicative function, $I[F(x_i) \leq u_i] = 1$,and $I[F(x_i) > u_i] = 0$. Assuming that the joint distribution copula function of u_i and v_i is $C(u_i, v_i)$, the squared Euclidean distance expression as follows.

$$d_{Gu} = \sum_{i=1}^{n} \left|\hat{C}(u_i, v_i) - C\left(u_i, v_i\right)\right|^2 \quad (6)$$

C. ESTIMATION OF THE PARAMETERS OF THE ACFs

After choosing the appropriate ACFs, it is also necessary to choose the appropriate parameter estimation method. For the N-element ACFs, since it is decomposed into N-1 binary ACFs, the parameter estimation of the multivariate ACFs can be transformed into the parameter estimation of the binary ACFs. The parameter estimation of the binary ACFs usually uses the maximum likelihood estimation (MLE) method, assuming that the marginal distribution functions of the variables x and y are $F(x, \theta_1)$, $G(y, \theta_2)$, and the density functions of these two marginal distribution functions are $f(x, \theta_1)$, $g(y, \theta_2)$, where θ_1 and θ_2 are two uncertain parameters, and the Copula function chosen is of the form $C(u, v, \alpha)$, and the corresponding density function as follows.

$$c(u, v, \alpha) = \frac{\partial^2 C(u, v, \alpha)}{\partial u \partial v} \quad (7)$$

The parameter α of the ACFs is indeterminate and the eq. (8) for the joint distribution function of the variables x and y as follows.

$$H(x, y, \theta_1, \theta_2, \alpha) = C\left[F(x, \theta_1), G(y, \theta_2), \alpha\right] \quad (8)$$

Its probability density function as follows.

$$\begin{aligned} h(x, y, \theta_1, \theta_2, \alpha) &= \frac{\partial^2 H}{\partial x \partial y} \\ &= c[F(x, \theta_1), G(y, \theta_2), \alpha] f(x, \theta_1) g(y, \theta_2) \end{aligned} \quad (9)$$

Therefore, for the sample $(x_i, y_i), i = 1, 2, \ldots, n$, the likely-hood function as follows.

$$\begin{aligned} L(\theta_1, \theta_2, \alpha) = \prod_{i=1}^{n} & c\left[F(x_i, \theta_1), G(y_i, \theta_2), \alpha\right] \\ & \times f(x_i, \theta_1) g(y_i, \theta_2) \end{aligned} \quad (10)$$

The target parameter estimate is computed by initially taking the logarithm of the aforementioned equation and subsequently determining the parameter value that results in a zero reciprocal, thereby yielding a maximum value.

$$\theta = \left(\hat{\theta}_1, \hat{\theta}_2, \hat{\alpha}\right) = \arg maxlnL(\theta_1, \theta_2, \alpha) \quad (11)$$

III. PATH PERFORMANCE DEPENDENT RELIABILITY MODELS FOR DISTRIBUTED NETWORKS

A. DELAY-BASED NETWORK PATH RELIABILITY DEFINITION

Following the path performance criteria developed by Professor Huang Ning [20], this paper places significant emphasis on network performance evaluation parameter, 'delay.' To achieve this, the delay data is first normalized and clustered, and subsequently, the delay distribution functions for each path are amalgamated into a collective distribution function for a family of paths. This is accomplished by constructing a delay-based distribution function using a multivariate composite ACFs. For the n-th path, denoted as L_n, K sampling points are taken within the time period t_1 to t_2, with a fixed sampling interval. The time delay at the i-th sampling point is recorded as $\tau_{L_{n,i}}$, and the K-means clustering algorithm is employed through iterative processes until convergence is reached in the time delay data. The resulting converged point serves as the time delay threshold $\tau_{L_n}^k$ (k indicates the number of delay thresholds), used in the subsequent reliability calculations. Consequently, the path performance failure rate is determined as the probability that the sampled delay value $\tau_{L_{n,i}}$ acquired over all sampling cycles for the path within the time period t_1 to t_2 is greater than or equal to the delay threshold $\tau_{L_n}^k$. Eq. (12) provides the probability density

function for the delay.

$$f\left(\tau_{L_{n,i}} \geq \tau_{L_n k}\right) = \frac{dF\left(\tau_{L_{n,i}} \geq \tau_{L_n}^k\right)}{d\tau} \tag{12}$$

The path performance reliability is given by the cumulative distribution function of the time delay as in eq. (13).

$$\begin{aligned} R\left(\tau_{L_n}\right) &= 1 - \int_{\tau_{L_{n,i}}}^{\max \tau_{L_{n,i}}} f\left(\tau_{L_{n,i}} \geq \tau_{L_n}^k\right) \\ &= 1 - F\left(\tau_{L_{n,i}} \geq \tau_{L_n}^k\right) \end{aligned} \tag{13}$$

where $max\tau_{L_{n,i}}$ refers to the maximum value of the path delay data collected on path n during the time period $t_1 - t_2$.

Then at the i-th sampling period, for any path L_n, the path unreliability is given by the cumulative distribution function of the path delay as follows.

$$U_{L_{n,i}} = F\left(\tau_{L_{n,i}} \geq \tau_{L_n}^k\right) \tag{14}$$

B. PATH FAMILY RELIABILITY MODELING BASED ON MULTIVARIATE ACFs

Two definitions for distributed path control systems are given in the following:

Definition 1: A family of parent node paths refers to the set of paths that send data from a particular parent node to more than one child nodes as in Fig. 1.

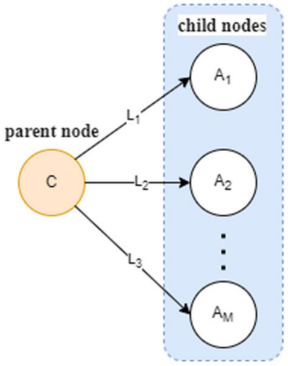

FIGURE 1. Path family of the parent node.

Definition 2: A family of child node paths means a collection of paths that send data from a different parent node to the same child node, as in Fig. 2.

In both of these sets of paths, the presence of a common parent node for all child nodes, or conversely, a common child node for all parent nodes, results in a scenario where interference sources in proximity to the child (parent) node, or device failures within the parent (child) node, can have a cascading effect on all paths linked to that particular parent (child) node due to the inherent correlation in path performance.

After introducing the Copula function, the cumulative distribution function of each path within the path family is combined to establish the joint distribution function, and the

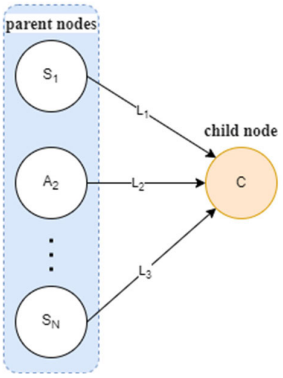

FIGURE 2. Path family of the child node.

unreliability of the parent node path family can be obtained according to eq. (15).

$$U_{parent} = C\left[F\left(\tau_{L_{1,i}} \geq \tau_{L_1}^k\right), \ldots, F\left(\tau_{L_{M,i}} \geq \tau_{L_M}^k\right)\right] \tag{15}$$

Thus, the delay-based reliability of the parent path family is calculated as follows.

$$\begin{aligned} R_{parent} &= 1 - U_{parent} \\ &= 1 - C\left[F\left(\tau_{L_{1,i}} \geq \tau_{L_1}^k\right), \ldots, F\left(\tau_{L_{M,i}} \geq \tau_{L_M}^k\right)\right] \end{aligned} \tag{16}$$

Similarly, the unreliability of the family of sub-node paths can be obtained according to eq. (17).

$$U_{child} = C\left[F\left(\tau_{L_{1,i}} \geq \tau_{L_1}^k\right), \ldots, F\left(\tau_{L_{N,i}} \geq \tau_{L_N}^k\right)\right] \tag{17}$$

The reliability of the sub-node path family as follows.

$$\begin{aligned} R_{child} &= 1 - U_{child} \\ &= 1 - C\left[F\left(\tau_{L_{1,i}} \geq \tau_{L_1}^k\right), \ldots, F\left(\tau_{L_{N,i}} \geq \tau_{L_N}^k\right)\right] \end{aligned} \tag{18}$$

C. RELIABILITY MODLING OF SUBSYSTEMS

A distributed NCS is shown in Fig. 3. A group of sensors such as S_{11}, S_{12} and S_{13} in the figure is called a sensor family (S_1), C_1, C_2 and C_3 are controllers and A_{11} and A_{12} are actuators.

Taking subsystem S_1 as an example, the specific information transfer pattern within the entire system is as follows: S_1 detects signals and transmits them to the controller node C_1 via the network. C_1 receives data from three sensors within its domain and computes control signals for different target actuator nodes. Subsequently, C_1 dispatches the respective control signals to actuator nodes A_{11} and A_{12}, effectively accomplishing the real-time control of the designated object.

In cases where the delay of the communication path from S_1 to C_1 surpasses the predefined threshold, the path is considered unsuccessful. In such instances, the data is rerouted to the controller with the next highest priority, according to the routing protocol. In this scenario, it is forwarded to the neighboring controller C_2, which in turn communicates with

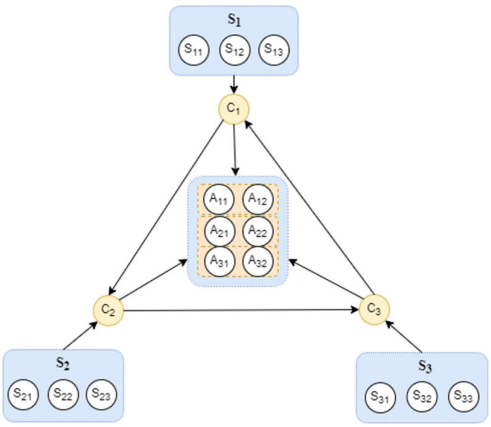

FIGURE 3. Distributed network control system transmission paths.

actuator nodes A_{11} and A_{12}. Should the delay of the path from S_1 to C_2 similarly exceed the specified threshold, the data is further forwarded to the adjacent controller C_3, which subsequently communicates with actuator nodes A_{11} and A_{12}. This sequential transmission process, encompassing the lower sensors, intermediary controllers, and upper-level actuators, collectively forms an autonomous subsystem referred to as 'subsystem C1'. The specific transmission path for this subsystem is illustrated in Fig. 4.

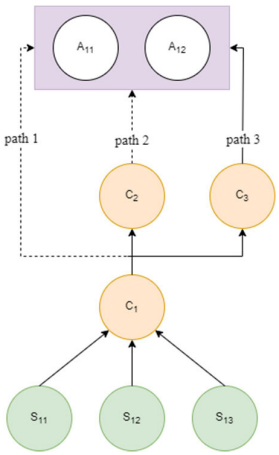

FIGURE 4. Transmission path of subsystem C1.

This particular subsystem can be further dissected into two distinct segments: a sub-node path family, encompassing the route from the sensors transmitting signals to the controller, and a parent path family, encapsulating the journey from the controller relaying signals to the actuators. Among these, the sensor-to-controller path family, depicted in Fig. 5, serves as an illustrative example of the sub-node path family.

The reliability of the model can be obtained by eq. (19) based on the multivariate composite ACFs for sub-nodes, where the symbol (S → C) indicates the signal from the sensor to the controller, the superscript k indicates the reliability

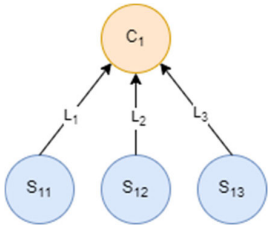

FIGURE 5. The sensor-controller path family of subsystem C1.

at the k-th delay threshold.

$$R^k_{(S\to C)} = 1 - C\left[F\left(\tau_{L_{1,i}} \geq \tau^k_{L_1}\right), \ldots, F\left(\tau_{L_{3,i}} \geq \tau^k_{L_3}\right)\right] \tag{19}$$

In contrast, the path family from the controller to the actuator in subsystem C1 has a multi-hop transmission mechanism, i.e., an unsuccessful transmission of one path will be transferred to another path for transmission, and its reliability calculation is relatively more complicated, and can be divided into nine different parent node path families. Fig. 6 shows the nine different parent node path families in subsystem C1 for signals sent from the controller to actuators A_{11} and A_{12}, where Ln indicates the signal transmission path.

Since in actual production operation, different actuators belonging to the same subsystem are in a relatively close environment, which results in the impact of external noise on the communication performance of the proximity path has relevant characteristics, and these actuators share the same set of network protocols and routing mechanisms at the network level, making it very rare for different actuators to have heterogeneous multi-hop transmission, and the impact of these cases on the reliability of the subsystem is very small, so they are often ignored in the actual calculation and not discussed specifically [21]. Therefore for the controller-to-actuator path family in subsystem C1, the reliability calculation can be simplified to consider only the coupling of the same multi-hop, i.e. parent node path families I, IV and IX, according to the full probability formula.

The reliability of each parent path family is denoted as $R_{(C\to A)_{m,n}}$, where (C→A) denotes the number of times the signal is sent from the controller to the actuator, m denotes the number of multi-hop transmissions the signal is sent to the first actuator A_{11}, and n denotes the number of multi-hop transmissions the signal is sent to the second actuator A_{12}.

The parent node path family I for controller C_1 is sent directly to actuator A_{11} and actuator A_{12} without multi-hop transmission and its reliability is expressed using the binary ACFs in eq. (20), where the subscript '00' would represent without multi-hop transmission and the superscript k indicates the reliability at the k-th delay threshold.

$$R^k_{(C\to A)_{00}} = 1 - C\left[F\left(\tau_{L_{4,i}} \geq \tau^k_{L_4}\right), F\left(\tau_{L_{5,i}} \geq \tau^k_{L_5}\right)\right] \tag{20}$$

The parent node path family IV represents the path family reliability of sensor C_1 sent to actuators A_{11} and A_{12} after one

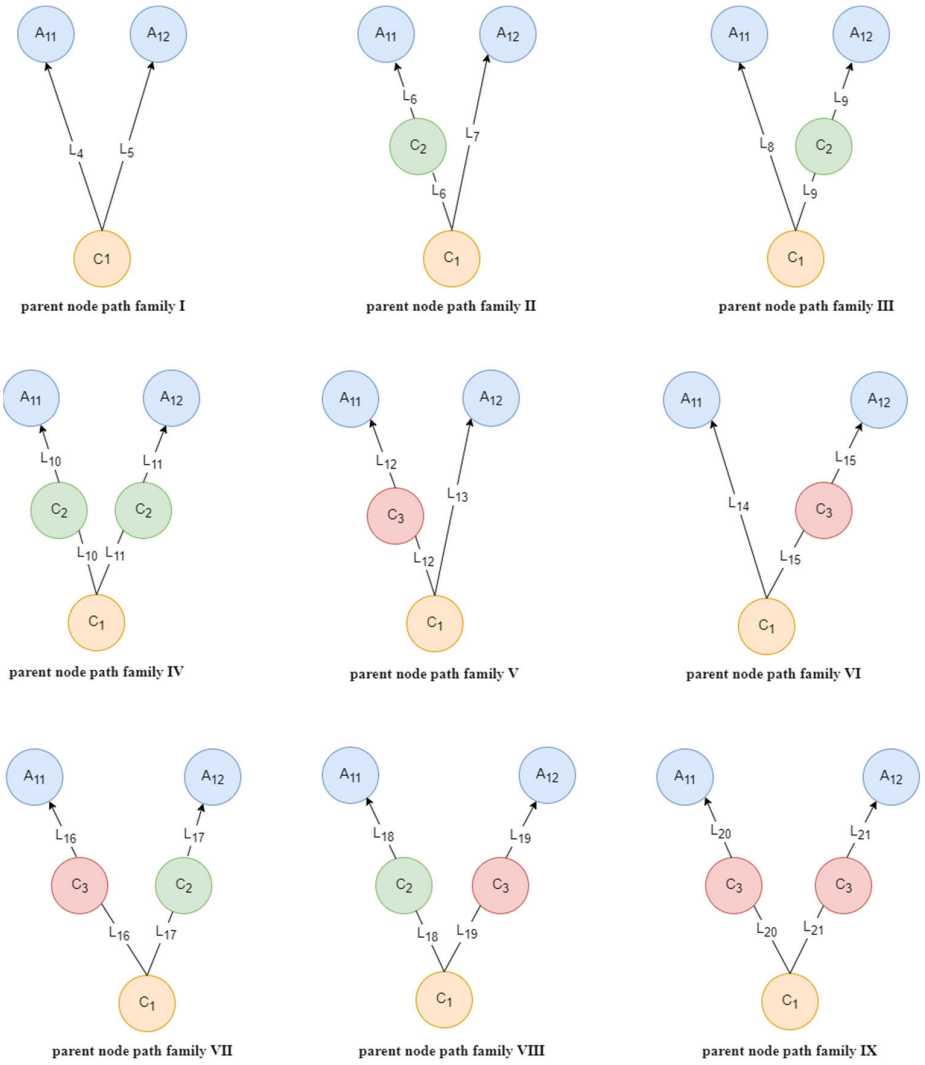

FIGURE 6. Controller - actuator path family of subsystem C1.

multi-hop, which can be expressed using the binary ACFs as follows.

$$R^k_{(C\to A)_{11}} = 1 - C\left[F\left(\tau_{L10,i} \geq \tau^k_{L10}\right), F\left(\tau_{L11,i} \geq \tau^k_{L11}\right)\right] \tag{21}$$

The parent node path family IX represents sensor C_1 sending packets to actuators A_{11} and A_{12} over two multi-hops, whose path family reliability can be expressed using the binary ACFs as follows.

$$R^k_{(C\to A)_{22}} = 1 - C\left[F\left(\tau_{L20,i} \geq \tau^k_{L20}\right), F\left(\tau_{L21,i} \geq \tau^k_{L21}\right)\right] \tag{22}$$

Then for the controller-to-actuator path family in subsystem C1, the reliability can be calculated according to the full probability formula as shown in eq. (23) when considering only the path families with simultaneous multi-stage jumps.

$$\begin{aligned} R^k_{(C\to A)} &= R^k_{(C\to A)_{00}} + \left(1 - R^k_{(C\to A)_{00}}\right)\cdot R^k_{(C\to A)_{11}} \\ &+\left[1 - R^k_{(C\to A)_{00}} - \left(1 - R^k_{(C\to A)_{00}}\right) R^k_{(C\to A)_{11}}\right]\cdot R^k_{(C\to A)_{22}} \end{aligned} \tag{23}$$

Therefore, the subsystem C1 reliability can be derived from the two-level path reliability as follows.

$$R^k_{subC1} = R^k_{(S\to C)} \cdot R^k_{(C\to A)} \tag{24}$$

D. RELIABILITY MODELING OF DISTRIBUTED NCSs

Based on the same principles, the reliability of the other two subsystems C2 and C3 of the distributed NCS shown in Fig. 3 can be obtained. For a distributed NCS, subsystems are equal, i.e. the failure of any subsystem will cause fail of whole system. Thus, for the distributed NCS shown in Fig. 3, the reliability of whole system is shown in eq. (25), with *n*denoting the reliability of *n*-th subsystem (n=1,2,3).

$$R^k_{sys} = R^k_{subC1} \cdot R^k_{subC2} \cdot R^k_{subC3} \tag{25}$$

Consequently, drawing upon the analyses presented in Chapters 1 and 2, a novel approach is formulated. This approach, implemented in the subsequent steps, leverages ACFs to assess the reliability of a distributed networked control system with respect to path performance.

Step 1: NCSs is segmented into multiple subsystems based on distinct functional modules, illustrated in Fig. 4. Within these subsystems, the two-level path families extending from sensors to controllers and from controllers to actuators are further divided into distinct parent node path families and child node path families in accordance with the definitions outlined in Chapter III, Section B. These path families are constituted by a multitude of information transmission paths.

Step 2: During the sampling period from t_1 to t_2, the delay data for each path L_n is collected with fixed sampling interval. The delay at the i-th sampling period of the n-th path is denoted as $\tau_{L_{n,i}}$. After noise reduction and standardization of the delay data using K-means clustering algorithm, the cohesion points $\tau_{L_n}^k$ of pre-processed data are iteratively determined. The values serving as a delay threshold for reliability evaluation is subsequently organized in ascending order.

Step 3: The pre-processed delay data for each path is fitted to an appropriate cumulative distribution function. Subsequently, the parameters of the distribution function are estimated, enabling the calculation of path reliability using eq. (13).

Step 4: The suitable ACF is selected by comparing the squared Euclidean distance d_{Gu} using eq. (6). Subsequently, the maximum likelihood estimation method, as defined in eq. (11), is applied to determine the correlation parameter for the selected ACF. Finally, the reliability of the parent and child node path families for path performance correlation is assessed based on eq. (16) and (18).

Step 5: Having determined the reliability for both the parent and child node path families, the reliability for the two-tier path families—spanning from sensors to controllers and from controllers to actuators within each subsystem is computed using the comprehensive probability eq. (23). Subsequently, the reliability of each subsystem is ascertained using eq. (24).

Step 6: Finally, the reliability of the entire distributed NCS is determined by multiplying the reliability of all subsystems, with the assumption of independence of subsystem as described in eq. (25).

IV. CASE STUDY OF RELIABILITY EVALUATION OF DISTRIBUTED NCSs

In this thesis, a distributed NCS consisting of three subsystems is established using OPNET network simulation software. This setup is employed to simulate random delay data within the wireless NCS during the information transmission process. The aim is to validate the reliability model that relies on ACF.

A. SYSTEM MODELING

OPNET is a versatile tool designed for modeling, simulating, and conducting performance analyses of computer networks. It enables the simulation of NCSs under various network environments and protocols. By gathering data that reflects network conditions, such as delays and packet loss rates in information transmission paths, it facilitates the evaluation of network performance. The OPNET simulation model is structured into three layers: the process layer, the node layer, and the network layer. Initially, the network topology is configured in the network layer, as illustrated in Fig. 7.

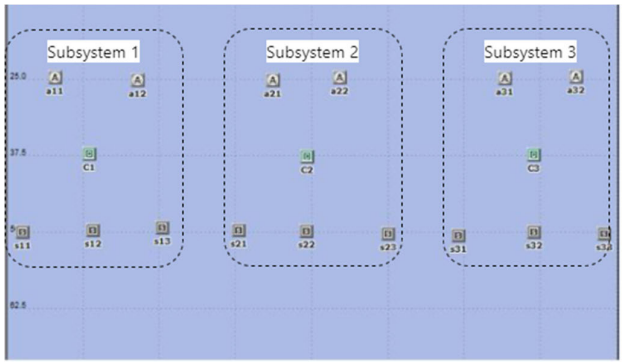

FIGURE 7. OPNET network layer model.

The model comprises three subsystems, with each subsystem having a sensor denoted as S_{ij} (j=1, 2, 3). These sensors are tasked with gathering signals and subsequently transmitting them to the respective controller C_i, within their respective subsystems. These controllers process the received signals and send computed control signals to the actuators, A_{ij} (j=1, 2), which are responsible for executing the necessary control operations.

Secondly, in the node layer, attributes are defined for each node within the network layer, representing various types of network nodes found in real physical networks. These nodes consist of different process modules used to replicate the communication and data exchange processes between devices in an actual network. For instance, let's consider the controller C_1. Its node layer model is structured as depicted in Fig. 8. In this model, the Source module is responsible for generating data packets and transmitting them to the Router module. The Router module, in turn, transmits signals to the MAC module for tasks such as configuring time slot lengths, encapsulating and dispatching frames, and more. Additionally, the Sink module is tasked with recording and tallying the delay information pertaining to data transmission.

Finally, the specific design and parameter configuration for each module within the node layer are conducted in the process layer individually. To illustrate, let's consider the network layer node C1. The process layer model for each module of its node layer is established as follows.

a) Source module: the process layer model is drawn as shown in Fig. 9, where Init is the initialization process, used to obtain node-related attributes; off is the stop state, indicating that no longer send data frames to the
b) outside world; on is the active state, in which the node generates data packets according to the set

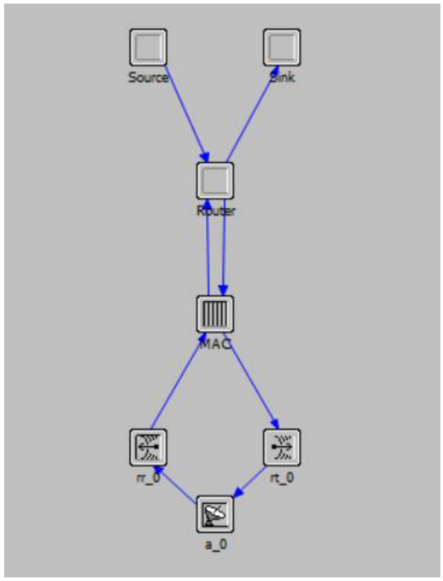

FIGURE 8. Node level model for controller C1.

requirements. The time interval for generating packets is set to 0.2 seconds, the size of each packet is 128bits, and the specific parameters of the module are shown in Table 1.

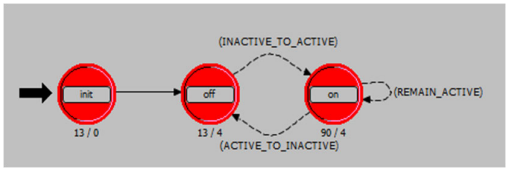

FIGURE 9. Process-level model of the source module.

TABLE 1. Source module parameters.

Packet Generation Arguments	Value
Interarrival Time (seconds)	Constant (0.2)
Packet Size (bits)	Constant (128)
Segmentation Size (bits)	No Segmentation

where Attribute denotes the variable name and Value denotes the variable value. The first variable Interarrival Time is set with a parameter of 1.0, indicating that the packet is sent every second. The second variable Packet Size, the parameter for packet size, is set to 1024bits, indicating that the size of the packet sent by the sensor to the target actuator every time is 1024bits.

c) Router Module: The process layer model for establishing the Router module is shown in Fig. 10, which is responsible for receiving signals generated by the Source module and then sending them to the actuator nodes of the system via the MAC module.

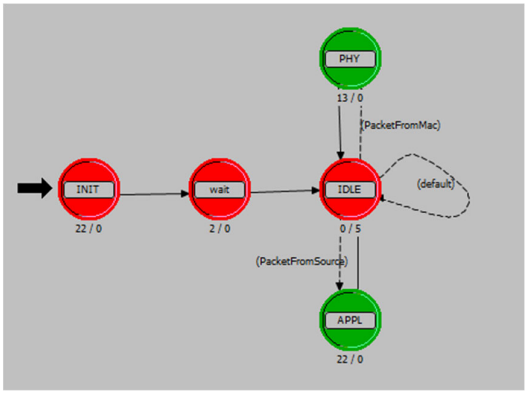

FIGURE 10. Process level model of the router module.

The specific process is that the data is initialized in the INIT region to obtain the relevant node attributes, and then wait for other data processes to complete the initialization through the Wait region, and then wait for interrupts to arrive by the IDLE, APPL receives the packets generated by the node layer Source and periodically sends the packets to the node layer of the MAC module, the PHY by identifying the destination address of the received packets, and then receives them when they match. and sends it to the Sink module for delay statistics, otherwise it destroys the data.

d) Sink module: the process layer model of the Sink module is shown in Fig. 11, which is mainly used to count the latency information of the data.

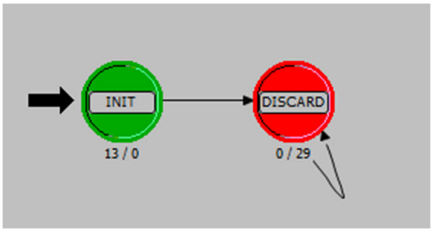

FIGURE 11. Process layer model of the MAC module.

Specifically, when the Sink module receives a packet, it will record the arrival timestamp, which indicates the arrival time of the packet, and at the same time, the packet also contains a send timestamp, which indicates the time when the packet leaves the previous node, and the Sink module uses the arrival timestamp to subtract the send timestamp to get the packet's transmission delay data.

e) MAC module: MAC module is known as the protocol module, the establishment of the process layer model is shown in Fig. 12.

The same INIT region is responsible for the initialization of the data, Wait indicates that the waiting region, and then IDLE wait for the interrupt to arrive, in this state nodes do not send data, but will allow the PHYPacket to receive the physical layer of the data packet and send it to the Router Routing Module, when their own time slot arrives, the jump

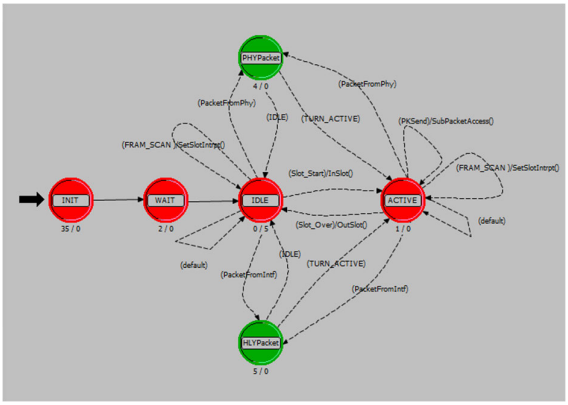

FIGURE 12. MAC module process level model.

to the ACTIVE state, in the ACTIVE state, indicating that the node is in their own time slots, to take out packets for sending.

B. SETTING OF SYSTEM NODE PARAMETERS

1) PARAMETERIZATION OF SENSOR NODES

Taking the sensor S_{11} in Fig. 7 as an example, its specific parameter settings are shown in Table 2.

TABLE 2. Parameters of sensor node S11.

Attribute	Value
name	S_{11}
Address	11
MAC.DataRate	64000
Router.DestAddress	1
Router.ExecuteAddr	promoted
Router.SrcType	promoted
Router.TrajecStatic	promoted
Start Time (seconds)	Constant (5.0)
ON State Time (seconds)	Constant (90.0)
OFF State Time (seconds)	Constant (1)
Interarrival Time (seconds)	Constant (0.2)
Packet Size (bits)	Constant (128)

The term "Address" denotes the network address of sensor node S11, which has been configured to 11. "MAC.DataRate" signifies the data transmission rate of the node, set at 64 kbps. "Start Time" indicates the initiation time of the service process. When the value is set to 5.0, the sensor node commences the service process five seconds after the overall service begins. The "ON State Time" of 90 seconds represents the duration during which the node remains in the active "ON" state. Similarly, "OFF State Time" designates the period for which the node remains in the "OFF" state, which is set to 1 second. "Interarrival Time" signifies the time interval for sending data packets, configured at 0.5 seconds. Finally, "Packet Size" indicates that each data packet has a size of 128 bits.

2) PARAMETERIZATION OF THE CONTROLLER

In the case of controller C1, as illustrated in Fig. 7, specific parameter configurations are detailed in Table 3.

TABLE 3. Parameter setting for controller node C1.

Attribute	Value
name	C_1
Address	1
MAC.DataRate	64000
Router.DestAddress	2
Router.NbrCt1	promoted
Router.T	promoted
Start Time (seconds)	Constant (5.0)
ON State Time (seconds)	Constant (90.0)
OFF State Time (seconds)	Constant (1)
Interarrival Time (seconds)	Constant (0.2)
Packet Size (bits)	Constant (128)

Similar to the meaning of the parameter representation in the sensor, where Adderss is the network address of C_1, which is set to 1; MAC.DataRate indicates the data transfer rate of this node, which is also set to 64kbps. Router.DestAddress refers to how many execution nodes the controller node needs to send data to. Start Time Indicates that the sensor node starts its service process 5 seconds after services start.

Using the same method, the remaining nodes in the network layer are designed for the node layer and process layer models, and the setting of relevant parameters is also completed, and then the system is simulated and delay data are collected. The statistics of delay is completed by the Sink module in the node layer, firstly, the end-to-end delay statistics need to be sounded in the node layer, as shown in orange in Table 4, and then it is added as a statistic variable in the network layer, and then the delay data collected by the system is exported at the end of the simulation.

TABLE 4. End-to-end delay statistics.

Orig. Name	Prom. Name
rr_0. channel [0].packet loss ratio	Packet loss ratio
rr_0. channel [0].bit error rate	Bit error rate
Sink.End-to-End Delay	End-to-End Delay (seconds)
rr_0.channel [0].throughput	Throughput (bits/sec)
rr_0.channel [0].throughput	Throughput (packet/sec)

The delay data from the sensor to the controller of the subsystems in the simulation model is shown in Fig. 13.

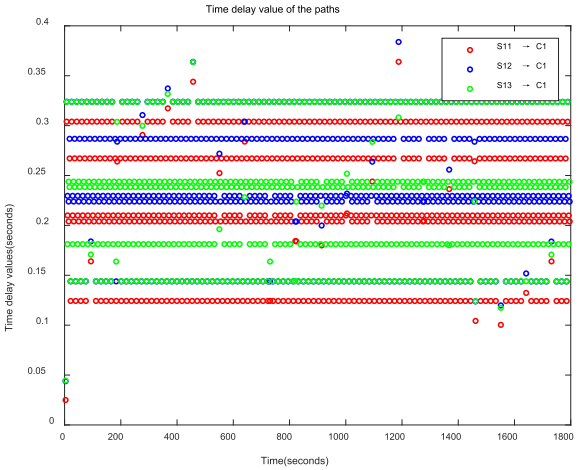

FIGURE 13. Sensor-controller path time delay sampling values for subsystem C1.

TABLE 5. Path delay thresholds for subsystem C1.

Path	$\tau_{L_n}^1$	$\tau_{L_n}^2$	$\tau_{L_n}^3$	$\tau_{L_n}^4$
$S_{11}\rightarrow C_1$	1.5654	0.2294	0.7232	1.3277
$S_{12}\rightarrow C_1$	1.5714	0.2384	0.7220	1.3372
$S_{13}\rightarrow C_1$	1.3463	0.7298	0.2369	1.5657
$C_1\rightarrow A_{11}$	1.5816	0.2400	0.7266	1.3459
$C_1\rightarrow A_{12}$	7.3232	1.3539	0.2790	1.0026
$C_1\rightarrow C_2\rightarrow A_{11}$	1.4540	0.6012	0.3134	1.4414
$C_1\rightarrow C_2\rightarrow A_{12}$	1.4540	0.6012	0.3134	1.4414
$C_1\rightarrow C_2\rightarrow C_3\rightarrow A_{11}$	1.4570	0.3102	0.6105	1.4431
$C_1\rightarrow C_2\rightarrow C_3\rightarrow A_{12}$	1.3709	0.0495	0.4805	1.1640

The simulation model comprises three subsystems. In conjunction with the information transmission methods outlined in the previous Section II-C, it becomes evident that the entire network system encompasses a total of 45 information transmission pathways. The transmission delays associated with these 45 information transmission paths have been gathered, using an experimental simulation duration of 1800 seconds and a sampling interval of 3.6 seconds. This collection process results in a total of 22,500 delay data points.

C. DATA PRE-PROCESSING

Firstly, it is essential to standardize the data as recommended in [22]. This involves subtracting the original delay data from the mean value of the delay data for each path and then dividing the result by the standard deviation of the delay data for that path. This process yields the standardized version of the original data.

Secondly, the standardized data was subjected to clustering using the K-means clustering algorithm, as described in [23] and [24]. The number of clusters, denoted as 'k' was initially set to 4, and four samples were chosen as the initial cluster centroids, commonly referred to as clustering seeds. Specifically, these seeds corresponded to the 100th, 200th, 300th, and 400th time delay data points in each dataset.

Through multiple iterations of the algorithm, these centroids were refined, and the resulting cluster centroids were employed as the time delay thresholds for subsequent reliability calculations. The four refined coalescence points for each path were arranged in ascending order, yielding the four time delay thresholds for each path, denoted as $\tau_{L_n}^1$, $\tau_{L_n}^2$, $\tau_{L_n}^3$ and $\tau_{L_n}^4$ respectively. The delay thresholds for all paths within subsystem C1 are presented in Table 5 as follows.

The presence of negative values in the table can be attributed to the normalization process. After data normalization, time delay data that fall below the mean are represented as negative values. It's important to note that the sign (positive or negative) of these values doesn't alter the intrinsic nature of the data or impact the subsequent calculations.

D. PATH PERFORMANCE RELIABILITY

According to eq. (13), the path's performance reliability is expressed through the cumulative distribution function of the delay. After preprocessing, the DISTRIBUTION FIT toolbox in MATLAB is employed to identify an appropriate cumulative distribution function and estimate its parameters. The most fitting cumulative distribution function is determined to be the first subtype of the Gumbel-type standard minimal value distribution within the extreme value distribution family, characterized by the cumulative distribution function described as follows.

$$F_n(x) = 1 - e^{(-e)^{\frac{x-\mu}{\sigma}}} \tag{26}$$

where μ, σ are the distribution parameters, μ is its location parameter, which is essentially the plurality of the distribution, and σ is the scale parameter, which is determined by the dispersion of the distribution, and both distribution parameters are unitless.

Table 6 lists the parameters of the Gumbel-type standard minimum value distribution for each path delay data in subsys-tem C1.

E. CALCULATE THE PATH FAMILY RELIABILITY

Once the cumulative distribution function for the time delay of each path is determined, we proceed to assess the reliability of each path family using multivariate ACFs. The process comprises two primary steps: first, the selection of appropriate ACFs and the estimation of their parameters; second, the computation of the path family's reliability.

1) SELECTION OF ACFs

Taking the sub-node path family from the sensor to the controller in subsystem C1 as an example, the edge distribution,

TABLE 6. Distribution parameters of subsystem C1.

Path	μ Position parameters	σ Scale Parameters
$S_{11}\rightarrow C_1$	0.4802	0.5471
$S_{12}\rightarrow C_1$	0.4825	0.8526
$S_{13}\rightarrow C_1$	0.5066	0.9581
$C_1\rightarrow A_{11}$	0.4448	0.7601
$C_1\rightarrow A_{12}$	0.4459	0.7622
$C_1\rightarrow C_2\rightarrow A_{11}$	0.4833	0.8855
$C_1\rightarrow C_2\rightarrow A_{12}$	0.4871	0.8956
$C_1\rightarrow C_2\rightarrow C_3\rightarrow A_{11}$	0.4878	0.8969
$C_1\rightarrow C_2\rightarrow C_3\rightarrow A_{12}$	0.4861	0.8977

represented as a Copula function, encompasses the cumulative distribution functions of time delay data from three paths. Specifically, let the cumulative distribution function of the $S_{11}\rightarrow C_1$ path delay be denoted as F_1, the cumulative distribution function of the $S_{12}\rightarrow C_1$ path delay as F_2, and the cumulative distribution function of the $S_{13}\rightarrow C_1$ path delay as F_3. To estimate the parameters of the binary distribution functions F_1 and F_2, the COPULA FIT function in MATLAB was employed, utilizing the maximum likelihood estimation method described in eq. (11). The parameter calculation results for these three commonly used ACFs are presented in Table 7.

TABLE 7. The first archimedes copula parameters.

Gumble	Clayton	Frank
157.4865	288.5971	23.16337

Upon determining the parameters for each ACF, sample empirical functions were generated following eq. (5), and subsequently, the squared Euclidean distances were computed as per eq. (6), as illustrated in Table 8.

TABLE 8. The first fitted squared euclidean distance.

Gumble	Clayton	Frank
0.9790	0.2072	0.2432

Following the principle that a smaller squared Euclidean distance indicates a better fit for the Archimedes Copula function, it becomes evident that the Clayton Copula should be selected to model the cumulative distribution function F_1 for the $S_{11}\rightarrow C_1$ path and the cumulative distribution function $F_2$for the $S_{12}\rightarrow C_1$ path. The corresponding fitting expression is presented in eq. (27).

$$C(F_1, F_2) = \left(F_1^{-288.5971} + F_2^{-288.5971}\right)^{\frac{1}{288.5971}} \tag{27}$$

According to the combination principle of ACFs shown in eq. (1), we can obtain eq. (28).

$$C(F_1, F_2, F_3) = C(C(F_1, F_2), F_3) \tag{28}$$

The second maximum likelihood parameter estimation was performed for $C(F_1, F_2)$ and F_3 and the results are shown in Table 9.

TABLE 9. The second archimedes copula parameters.

Gumble	Clayton	Frank
3.4965	3.5537	10.3654

Following the computation of parameters for each ACF, a sample empirical function was constructed in accordance with eq. (5), and the squared Euclidean distance was subsequently calculated based on this sample empirical function, as displayed in Table 10.

TABLE 10. The second fitted squared euclidean distance.

Gumble	Clayton	Frank
0.6722	1.0140	0.6546

Adhering to the principle that a smaller squared Euclidean distance signifies a superior fit for the ACFs, it is evident that the Frank Copula should be selected for the fitting, as outlined in eq. (29).

$$\begin{aligned} &C(F_1, F_2, F_2) \\ &= \frac{1}{-10.3654} \\ &\quad \times \ln\left[1 + \frac{\left(e^{-10.3654C(F_1,F_2)} - 1\right)\left(e^{-10.3654F_3-1}\right)}{e^{-10.3654} - 1}\right] \end{aligned} \tag{29}$$

Employing the algorithm described above, the parameters of each path's ACFs are derived through maximum likelihood parameter estimation. Subsequently, the sample empirical function is utilized to calculate the squared Euclidean distance, aiding in the identification of the optimal ACFs for each path family. The preferred Archimedean function and its associated parameter values within subsystem C1 are presented in Table 11.

The entry $(S_{11}, S_{12})\rightarrow C_1$ in the table signifies the paths taken by sensor S_{11} and sensor S12 to transmit data to controller C_1. On the other hand, $((S_{11}, S_{12}), S_{13})\rightarrow C_1$ indicates that the data sent from sensor S_{11} and sensor S_{12} to

TABLE 11. Subsystem C1 path family optimal ACFs and its parameters.

Path family	ACFs	Parameter value
$(S_{11}, S_{12}) \rightarrow C_1$	Clayton	288.5971
$((S_{11}, S_{12}), S_{13}) \rightarrow C_1$	Frank	10.3654
$C_1 \rightarrow (A_{11}, A_{12})$	Frank	24.1775
$C_1 \rightarrow C_2 \rightarrow (A_{11}, A_{12})$	Clayton	197.5695
$C_1 \rightarrow C_2 \rightarrow C_3 \rightarrow (A_{11}, A_{12})$	Frank	5.5087

controller C_1 are initially analyzed and combined into a joint distribution function using a Copula function. Subsequently, a second Copula function is chosen, and the corresponding parameters are estimated, incorporating the path of sensor S_{13} transmitting data to C_1.

2) PATH FAMILY RELIABILITY BASED ON MULTIVARIATE ACFs

The reliability of all path families is computed for four distinct time delay thresholds using the parent and child path family reliability formulas presented in eq. (16) and (18), as depicted in Table 12 and Table 13.

Based on the results of path family reliability calculations in Table 12, it is evident that the reliability of each path family exhibits an upward trend as the delay threshold increases. This trend is particularly pronounced in the fourth threshold level, where path family reliability surpasses 0.9. This observation underscores that the paths demonstrate improved performance when suitable delay thresholds are chosen.

TABLE 12. Sensor to controller path family reliability.

Path family	$R^1_{(S\rightarrow C)}$	$R^2_{(S\rightarrow C)}$	$R^3_{(S\rightarrow C)}$	$R^4_{(S\rightarrow C)}$
$(S_{11}, S_{12}, S_{13}) \rightarrow C_1$	0.623	0.729	0.913	0.991
$(S_{21}, S_{22}, S_{23}) \rightarrow C_2$	0.649	0.800	0.886	0.979
$(S_{31}, S_{32}, S_{33}) \rightarrow C_3$	0.615	0.744	0.878	0.908

F. RELIABILITY CALCULATION OF SUBSYSTEMS

Following the determination of path family reliabilities within the system, the subsequent step involves calculating the reliability of each subsystem across four distinct delay thresholds as per eq. (24). These results are presented in Table 14, where the subscript n denotes the reliability of n-th subsystem.

To facilitate observation of changes in subsystem reliability at each time delay threshold, the data in table 10 are plotted as a line graph as shown in Fig. 14.

TABLE 13. Controller to actuator path family reliability.

Path family	$R^1_{(C\rightarrow A)}$	$R^2_{(C\rightarrow A)}$	$R^3_{(C\rightarrow A)}$	$R^4_{(C\rightarrow A)}$
$C_1 \rightarrow (A_{11}, A_{12})$	0.606	0.711	0.898	0.985
$C_1 \rightarrow C_2 \rightarrow (A_{11}, A_{12})$	0.110	0.259	0.563	0.943
$C_1 \rightarrow C_2 \rightarrow C_3 \rightarrow (A_{11}, A_{12})$	0.128	0.379	0.564	0.902
$C_2 \rightarrow (A_{21}, A_{22})$	0.001	0.191	0.531	0.944
$C_2 \rightarrow C_3 \rightarrow (A_{21}, A_{22})$	0.141	0.244	0.360	0.858
$C_2 \rightarrow C_3 \rightarrow C_1 \rightarrow (A_{21}, A_{22})$	0.698	0.847	0.937	0.991
$C_3 \rightarrow (A_{31}, A_{32})$	0.081	0.358	0.758	0.936
$C_3 \rightarrow C_1 \rightarrow (A_{31}, A_{32})$	0.638	0.784	0.929	0.942
$C_3 \rightarrow C_1 \rightarrow C_2 \rightarrow (A_{31}, A_{32})$	0.713	0.890	0.913	0.991

TABLE 14. Reliability of each subsystem.

Subsystems	R^1_{subCn}	R^2_{subCn}	R^3_{subCn}	R^4_{subCn}
C1	0.432	0.632	0.895	0.983
C2	0.453	0.678	0.830	0.971
C3	0.439	0.662	0.802	0.901

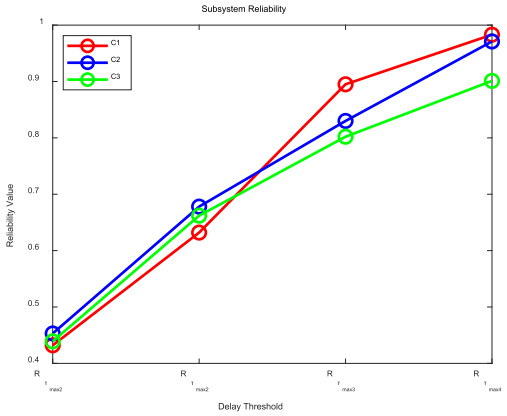

FIGURE 14. Reliability of each subsystem.

G. CALCULATE THE RELIABILITY OF THE WHOLE SYSTEM

After calculating the subsystem reliability, the distributed NCS reliability based on path performance correlation at four delay threshold levels can be evaluated based on the independence of subsystem actions. Bringing each subsystem reliability value into eq. (25), the system reliability is shown in Table 15.

TABLE 15. Reliability of the whole system.

R_{sys}^1	R_{sys}^2	R_{sys}^3	R_{sys}^4
0.086	0.086	0.596	0.860

Similarly, the data from Table 15 are plotted as show in Fig. 15.

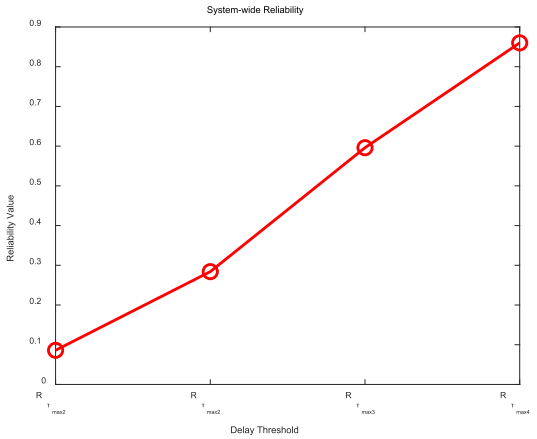

FIGURE 15. Reliability of the whole system.

As evident from Table 14, among the three subsystems, Subsystem C1 exhibits the highest reliability, whereas Subsystem C3 demonstrates overall poor reliability performance. In practical operations, increased frequency of daily inspections is advisable for Subsystem C3, given its suboptimal reliability. Real-time dynamic monitoring of the reliability of these subsystems is crucial, enabling timely maintenance actions when reliability warnings fall below the threshold necessary for the system's normal operation.

V. CONCLUSION

In this paper, time delay has been selected as the evaluation metric for path performance. The paper presents a definition of path performance reliability that is rooted in time delay and offers a methodology for calculating the cumulative distribution function of time delay. Building upon this foundation, the Archimedes Copula function is introduced as a means to assess the influence of path performance correlations on system reliability from a data-driven perspective.

Utilizing parameter estimation from the binary ACFs, we developed the multivariate composite ACFs and their corresponding parameter estimation method based on combination principles. Subsequently, a joint distribution function model for path family time delays is established. This model enables the development of a reliability calculation method for both sub-node path families and parent node path families. Furthermore, it facilitates the derivation of reliability assessments for the subsystem and the entire system.

The primary challenge in this paper lies in developing a comprehensive reliability evaluation model for distributed NCSs with the consideration of path performance correlations. This paper focuses only on time delay data as the source of network performance evaluation to assess the reliability of NCSs. By judiciously and effectively incorporating multiple performance indicators, such as packet loss rate, bit error rate, and others, into the evaluation framework, there is one significant potential for establishing a comprehensive network performance reliability assessment model, which would be a valuable avenue for future research.

The architecture of networked control systems with a multitude of diverse information transfer paths is inherently complex. This complexity will further increase sharply when it comes to the extension of network capacity, as well as considers the influence of uncertain data and dynamic environments at the same time. As demonstrated in this paper, focusing solely on path-based modeling can lead to computational challenges. Therefore, it is prudent to consider alternative approaches, such as network modeling techniques, which is specialized in dealing with the case of complex netwo-rk. For example, leveraging Bayesian modeling to construct a probabilistic system model and subsequently ascer-taining model parameters for reliability analysis might offer a promising avenue for future investigations.

REFERENCES

[1] N. G. Praveena and H. Prabha, "An efficient multi-level clustering approach for a heterogeneous wireless sensor network using link correlation," *EURASIP J. Wireless Commun. Netw.*, vol. 2014, no. 1, pp. 1–10, Dec. 2014.

[2] B. Chen, G. Hu, D. W. C. Ho, and L. Yu, "Distributed estimation and control for discrete time-varying interconnected systems," *IEEE Trans. Autom. Control*, vol. 67, no. 5, pp. 2192–2207, May 2022.

[3] E. Winfree, "Algorithmic self-assembly of DNA," California Inst. Technol., Pasadena, CA, USA, Tech. Rep. 4281288, 1998, pp. 33–34.

[4] W. K. Paul and E. W. Rothemund, "The program-size complexity of self-assembled squares," in *Proc. 32nd Annu. ACM Symp. Theory Comput.*, Chicago, IL, USA, 2020, pp. 727–737.

[5] L. Adleman, Q. Cheng, A. Goel, M.-D. Huang, D. Kempe, P. M. de Espanés, and P. W. K. Rothemund, "Combinatorial optimization problems in self-assembly," in *Proc. 34th Annu. ACM Symp. Theory Comput.*, May 2002, pp. 23–32.

[6] K. Srinivasan, M. Jain, J. I. Choi, T. Azim, E. S. Kim, P. Levis, and B. Krishnamachari, "The k factor: Inferring protocol performance using inter-link reception correlation," in *Proc. 16th Annu. Int. Conf. Mobile Comput. Netw.*, Sep. 2010, pp. 317–328.

[7] A. Khreishah, I. M. Khalil, and J. Wu, "Universal opportunistic routing scheme using network coding," in *Proc. 9th Annu. IEEE Commun. Soc. Conf. Sensor, Mesh Ad Hoc Commun. Netw. (SECON)*, Jun. 2012, pp. 353–361.

[8] G. Haylett, Z. Jadidi, and K. N. Thanh, "System-wide anomaly detection of industrial control systems via deep learning and correlation analysis," in *Proc. 17th Int. Conf. Artif. Intell. Appl. Innov.*, 2021, pp. 362–373.

[9] S. Yang, H. Jo. K. Lee, and I. Lee, "Expected system improvement (ESI): A new learning function for system reliability analysis," *Rel. Eng. Syst. Saf.*, vol. 222, pp. 1–14, Jun. 2022.

[10] X. Yuqin, Z. Yang, and D. Zhihui, "Distribution network power supply reliability prediction based on nonparametric kernel density estimation and Copula function," *J. North China Electr. Power Univ., Natural Sci. Ed.*, vol. 44, no. 6, pp. 14–19, Jun. 2017.

[11] Y. Liu and Y. Chen, "Dynamic reliability evaluation of high-speed train gearbox based on copula function," *IEEE Access*, vol. 10, pp. 51792–51803, 2022.

[12] H. An, H. Yin, and F. He, "Analysis and application of mechanical system reliability model based on copula function," *Polish Maritime Res.*, vol. 23, no. s1, pp. 187–191, Oct. 2016.
[13] S. Zoppi, S. P. Shantharam, and W. Kellerer, "Delay-reliability model of industrial WSN for networked control systems," in *Proc. IEEE Global Commun. Conf.*, Taipei, Taiwan, Dec. 2020, pp. 1–7.
[14] J. Shi, Y. Meng, S. Wang, and Z. Jiao, "A dynamic delay-based reliability evaluation model for communication networks," *Commun. Statist.-Simul. Comput.*, vol. 49, no. 6, pp. 1397–1414, Jun. 2020.
[15] S. Liang, Y. Wang, X. Bao, and J. Shi, "Reliability analysis of networked control systems considering data link performance correlation," in *Proc. 12th Int. Conf. Qual., Rel., Risk, Maintenance, Saf. Eng.*, Emeishan, China, ul. 2022, pp. 424–432.
[16] Y. Sei, J. A. Onesimu, and A. Ohsuga, "Machine learning model generation with copula-based synthetic dataset for local differentially private numerical data," *IEEE Access*, vol. 10, pp. 101656–101671, 2022.
[17] M. Dehghani, B. Saghafian, and M. Zargar, "Probabilistic hydrological drought index forecasting based on meteorological drought index using Archimedean copulas," *Hydrol. Res.*, vol. 50, no. 5, pp. 1230–1250, Oct. 2019.
[18] Z. Wang, J. Wang, P. Meng, F. Wang, and W. Dai, "Evaluation for parachute reliability based on fiducial inference and Bayesian network," in *Proc. Int. Conf. Math., Modeling, Simulation Statist. Appl. (MMSSA)*, Shang Hai, China, 2019, pp. 124–127.
[19] D. Yi and M. Rongyong, "Application comparison of different Copula functions in joint distribution of flood peak volume," *Water Power*, vol. 44, no. 12, pp. 24–26. Dec. 2018.
[20] H. Ning and W. Zhitao, "Review of network reliability evaluation models and algorithms," *Syst. Eng. Electron.*, vol. 35, no. 12, pp. 2651–2660, Dec. 2013.
[21] F. Jianming and X. Bingqiang, "A rolling time domain fusion estimation strategy for distributed network systems with packet loss," *Complex Syst. Complex. Sci.*, vol. 18, no. 3, pp. 75–79. Sep. 2021.
[22] Y. Fukami, "Standardization procedure for data exchange," *Information*, vol. 11, no. 6, p. 339, Jun. 2020.
[23] Z. Le, Z. En, Q. Leiyong, and Li Gongli, "Multi-party privacy protection k-means clustering scheme based on blockchain," *J. Comput. Appl.*, vol. 42, no. 12, pp. 3801–3812, Dec. 2022.
[24] M. Raeisi and A. B. Sesay, "A distance metric for uneven clusters of unsupervised K-means clustering algorithm," *IEEE Access*, vol. 10, pp. 86286–86297, 2022.

LONGHANG HUANG received the B.S. degree from the Chongqing University of Technology, in 2021. He is currently pursuing the M.S. degree in electronic information with the Inner Mongolia University of Technology. His main research interests include fault diagnosis and reliability analysis of distributed network control systems.

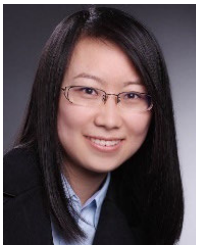

YING WANG received the B.S. degree in measurement and control technology and instrumentation from the China University of Mining and Technology, in 2007, the M.S. degree, in 2009, and the Ph.D. degree from the Institute of Electronic and Information Engineering, University of Duisburg–Essen, Germany, in 2014. She has been an Associate Professor with the School of Mechanical Engineering, Inner Mongolia University of Technology, China, since 2014. Her main research interests include signal acquisition and information processing, fault diagnosis, and reliability analysis of network control systems.

SHENG LIANG received the master's degree in electronic information from the Inner Mongolia University of Technology, in 2022. He has published several papers in international reliability conferences. His main research interest includes reliability evaluation of networked control systems based on Copula function.